Synthesis and Discovery of High Affinity Folate Receptor-Specific Glycinamide Ribonucleotide Formyltransferase Inhibitors with Antitumor Activity

Yijun Deng,[‡] Yiqiang Wang,[†] Christina Cherian,[||] Zhanjun Hou,[||] Steven A. Buck,[⊥] Larry H. Matherly,*[,‡,||,§,#] and Aleem Gangjee*[,†,#]

Graduate Program in Cancer Biology, Wayne State University School of Medicine, Detroit, Michigan 48201, Division of Medicinal Chemistry, Graduate School Pharmaceutical Sciences, Duquesne University, Pittsburgh, Pennsylvania 15282, Department of Pharmacology, Wayne State University School of Medicine, Detroit, Michigan 48201, Developmental Therapeutics Program, Barbara Ann Karmanos Cancer Institute, Detroit, Michigan 48201, and Department of Pediatrics, Children's Hospital of Michigan, Detroit, Michigan 48201

6-Substituted classical pyrrolo[2,3-*d*]pyrimidine antifolates with a three- to six-carbon bridge between the heterocycle and the benzoyl-L-glutamate (compounds **2**−**5**, respectively) were synthesized starting from methyl 4-formylbenzoate and a Wittig reaction with the appropriate triphenylphosphonium bromide, followed by reduction and conversion to the α-bromomethylketones. Cyclocondensation of 2,4-diamino-4-oxopyrimidine with the α-bromoketones, coupling with diethyl-L-glutamate, and saponification afforded **2**−**5**. Compounds **2**−**5** had negligible substrate activity for RFC but showed variably potent (nanomolar) and selective inhibitory activities toward Chinese hamster ovary cells that expressed FRα or FRβ and toward FRα-expressing KB and IGROV1 human tumor cells. Inhibition of KB cell colony formation was also observed. Glycinamide ribonucleotide formyl transferase (GARFTase) was identified as the primary intracellular target of the pyrrolo[2,3-*d*]pyrimidines. The combined properties of selective FR targeting, lack of RFC transport, and GARFTase inhibition resulting in potent antitumor activity are unprecedented and warrant development of these analogues as antitumor agents.

Introduction

Folates are members of the B class of vitamins that are cofactors for the synthesis of nucleotide precursors, serine, and methionine in one-carbon transfer reactions.[1] Since mammals cannot synthesize folates de novo, cellular uptake of these derivatives is essential for cell growth and tissue regeneration. Reflecting their hydrophilic anionic character, folates do not cross biological membranes by diffusion alone. Accordingly, mammalian cells have evolved sophisticated membrane transport systems to facilitate accumulation of folates.[2]

The ubiquitously expressed reduced folate carrier (RFC[a]) is the major transport system for folates in mammalian cells and mediates concentrative uptake of folate substrates.[2,3] RFC is a member of the major facilitator superfamily of transporters and is an integral transmembrane protein with micromolar affinity for its physiologic substrate, 5-methyl tetrahydrofolate. Importantly, RFC is also the primary transporter of clinically relevant antifolate drugs used for cancer including methotrexate (MTX),

raltitrexed (RTX), and pemetrexed (PMX) (Figure 1), and loss of RFC levels or function is a common mode of antifolate resistance.[3,4] While a previously unrecognized proton-coupled folate transporter (PCFT) was recently reported to contribute to folate absorption in the duodenum,[5] its tissue specificity and overall role in folate homeostasis are not yet clear.

The family of folate receptors (FRs) represents yet another mode of folate uptake into mammalian cells.[2,6,7] The FRs are high affinity folate binding proteins encoded by three distinct genes, designated α, β and γ, localized to chromosome 11q13.3−q13.5.[8] Another FR gene, designated γ, maps at chromosome 11q14.[9] FRs α, β, and γ are highly homologous proteins (68−79% identical amino acid sequence) and contain from 229 to 236 amino acids with two (β, γ) or three (α) N-glycosylation sites.[6] In contrast to RFC and PCFT, FRα and FRβ are anchored in plasma membranes by a glycosyl phosphatidylinositol (GPI) anchor. FRγ contains no GPI anchor and is secreted. Whereas FRα and FRβ (but not FRγ) mediate cellular accumulation of folate at low (nanomolar) concentrations by receptor-mediated endocytosis, these homologous proteins show differences in binding affinities for reduced folate substrates.[10]

The high affinity FRs offer a potential means of selective tumor targeting, given their restricted pattern of tissue expression and function.[6] For instance, FRα is expressed on the apical membrane surface of normal tissues such as kidney, placenta, and choroid plexus, whereas FRβ is expressed in placenta, spleen, and thymus. Importantly, FRα is overexpressed in a number of carcinomas including up to 90% of ovarian cancers.[11,12] Close associations were reported between FRα expression levels with grade and differentiation status of ovarian tumors. FRα in normal tissues (unlike tumors) is reported to be inaccessible to the circulation.[6] FRβ is expressed in a wide range of myeloid leukemia cells.[13] FRβ in normal hematopoetic cells differs from that in leukemia cells in its inability to bind folate ligand.[14]

* To whom correspondence should be addressed. For L.H.M.: phone, 313-578-4280; fax, 313-578-4287; e-mail, matherly@kci.wayng.edu. For A.G.: phone, 412-396-6070; fax, 412-396-5593; e-mail, gangjee@duq.edu.
‡ Graduate Program in Cancer Biology, Wayne State University School of Medicine.
† Duquesne University.
|| Barbara Ann Karmanos Cancer Institute.
⊥ Children's Hospital of Michigan.
§ Department of Pharmacology, Wayne State University School of Medicine.
# These authors contributed equally to this work.
a Abbreviations: RFC, reduced folate carrier; FRs, folate receptors; GARFTase, glycinamide ribonucleotide formyl transferase; MTX, methotrexate; RTX, raltiterxed; PMX, pemetrexed; TMQ, trimetrexate; PCFT, proton-coupled folate transporter; GPI, glycosyl phosphatidylinositol; LMX, lometrexol; TS, thymidylate synthase; DHFR, dihydrofolate reductase; CHO, Chinese hamster ovary; GAR, glycinamide ribonucleotide; FGAR, formyl glycinamide ribonucleotide; AICAR, 5-amino-4-imidazolecarboxamide ribonucleotide; FAICAR, formyl 5-amino-4-imidazolecarboxamide ribonucleotide; LCV, leucovorin.
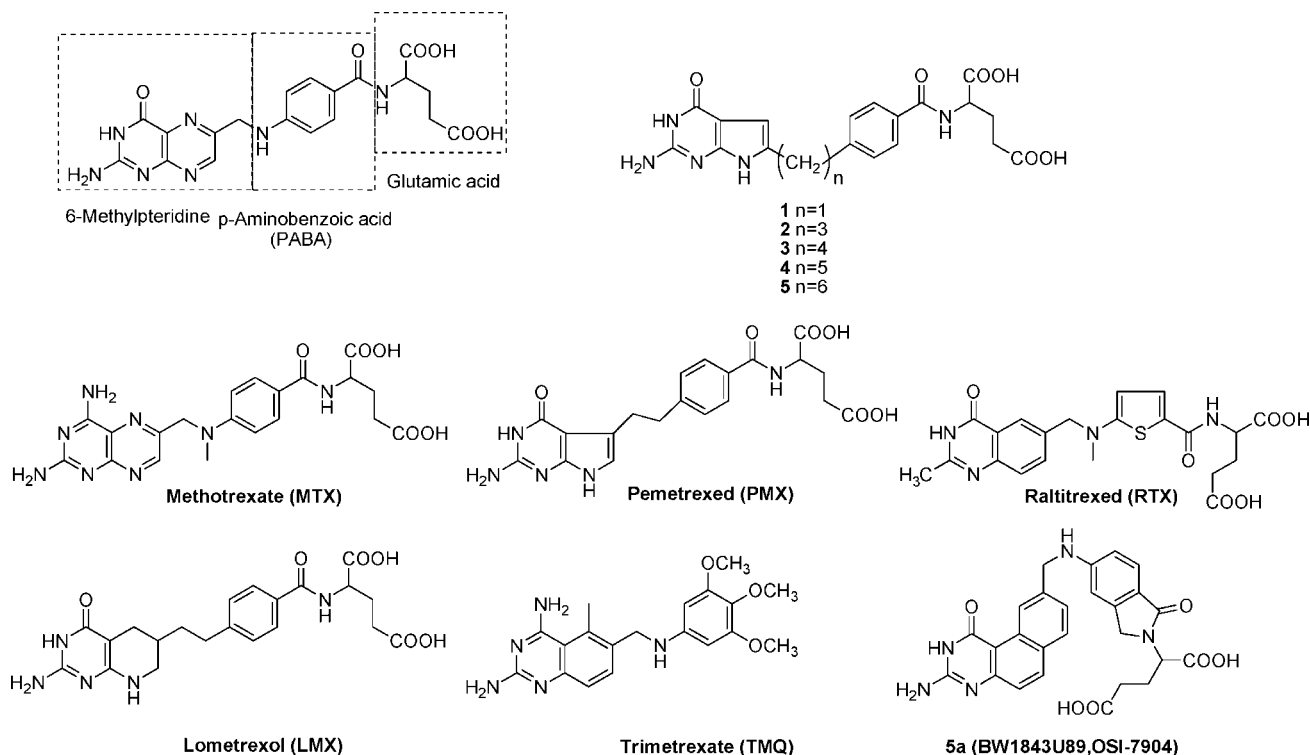
Figure 1. Folate and antifolate structures. Structures are shown for folic acid, depicting the pteridine, *p*-aminobenzoate, and glutamate motifs, along with structures for classical antifolates MTX, PMX, RTX, LMX, and **5a** (BW1843U89, OSI-7904) and the nonclassical antifolate trimetrexate (TMQ). In addition, the structures of the 6-substituted pyrrolopyrimidine antifolate series (**1**−**5**) are shown, as described in the text.

The concept of targeting FRs in cancer is not in itself new. Folate-conjugated cytotoxins, liposomes, radionuclides, or cytotoxic antifolates[6,7,15,16] have all been used to target FRs. Unfortunately, for most folate-based therapeutics such as *classical* antifolates [including RTX, PMX, and lometrexol (LMX)], tumor selectivity is lost, since substrates are shared between FRs and the ubiquitously expressed RFC. Indeed, this likely explains the severe myelosuppression encountered in phase 1 studies with LMX.[17]

One strategy for selectively targeting tumor cells via FRs involves prodrug conjugates in which folate or pteroate is covalently linked to cytotoxins such as mitomycin C[18] that, upon internalization, are selectively cleaved to release cytotoxic drug. While these drug conjugates are unlikely to be RFC substrates, the success of this tumor targeting approach could be significantly compromised by inefficient cleavage and release of the cytotoxic moiety, resulting in decreased chemotherapeutic activity. Alternatively, premature cleavage of the conjugates (prior to tumor internalization) could decrease selectivity and increase toxicity to normal proliferating tissues. In addition, use of folic acid conjugates could ultimately release free folic acid within the tumor which could function as a nutrient for the tumor. If, however, a FR-targeted ligand were *itself cytotoxic without RFC activity*, selective tumor targeting would ensue. Antifolates that selectively target FRs over RFC have been described[15] and, more recently, cyclopenta[*g*]quinazoline antifolates,[19,20] all of which potently inhibit thymidylate synthase (TS) within cells. When tested in mice,[20] one cyclopenta[*g*]quinazoline antifolate had no toxicity to normal tissues, as reflected in weight loss, nor were there any macroscopic signs of toxicity to major organs, consistent with the premise that FR targeting is highly selective.

On the basis of the clinical success of PMX and the lack of in vitro activity of the 6-regioisomer of PMX,[21] Gangjee et al.[22,23]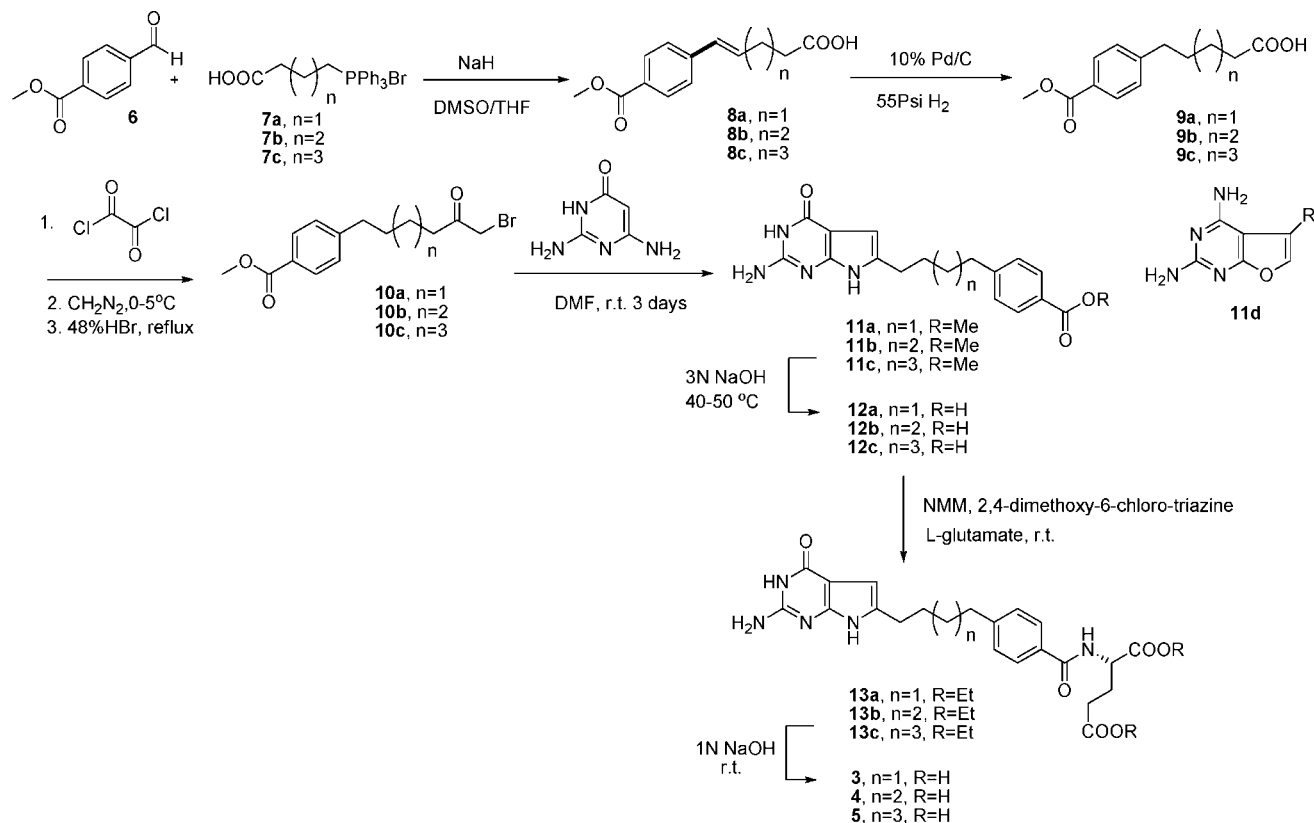 designed and synthesized classical 6-substituted 2-amino-4-oxopyrrolo[2,3-*d*]pyrimidine antifolates with three- and four-carbon bridges as inhibitors of dihydrofolate reductase (DHFR) and/or TS. Both of these compounds (**2** and **3**, respectively; Figure 1) were poor inhibitors of purified human DHFR and TS and were only modest inhibitors of CCRF-CEM leukemia cell growth in the presence of supraphysiologic folate which was largely protected by hypoxanthine (but not thymidine).[22,23] We now report that compounds **2** and **3**, along with their five- and six-carbon bridge homologues (**4** and **5**, respectively) (Figure 1), are selective high affinity ligands for FRs α and β with potent inhibitory activity against FR-expressing Chinese hamster ovary (CHO) and human tumor cells. We further identified the folate-dependent purine biosynthetic enzyme, glycinamide ribonucleotide formyltransferase (GARFTase), as the major intracellular target responsible for the cytotoxic activity of this class of agents. While antifolates that target GARFTase including LMX have been described[24] and are under continued development, to our knowledge, this is the first report of GARFTase inhibitors that are selectively transported into cells by FRs but not RFC and that exhibit potent inhibitory activities against FR-expressing tumor cells.

Chemistry

The synthesis of compounds **1**[25] and **2**, the one- and three-carbon bridged analogues, respectively, was accomplished as previously reported.[22,25] Compounds **3**−**5** were synthesized in this study using modifications of our previous method[22,23] reported for **2** and **3** (modifications discussed below).

Compounds **3**−**5** were obtained starting from the commercially available methyl 4-formylbenzoate (**6**) using an α-bromomethyl ketone condensation with 2,6-diamino-4-oxopyrimidine as the key step as outlined in Scheme 1. In the previous synthesis,[22,23] we used the α-chloromethylketones which afford both the 6-substituted pyrrolo[2,3-*d*]pyrimidine, as well as the 5-substituted furo[2,3-*d*]pyrimidine and involves

Scheme 1

a separation of the two compounds. In this study we elected to use the α-bromomethylketones which have been reported[26] to afford regiospecifically similar 6-substituted pyrrolo[2,3-*d*]pyrimidines without furo[2,3-*d*]pyrimidines. Thus, a Wittig reaction[27] of **6** with triphenylphosphonium bromides **7a−c** in 1:1 DMSO/THF with 2 equiv of NaH in an ice bath and N_2 atmosphere afforded the unsaturated acids **8a−c** as a mixture of *E*- and *Z*-isomers. Hydrogenation of **8a−c** afforded the saturated acids **9a−c**, which were converted to the acid chlorides and immediately reacted with diazomethane followed by 48% HBr to give the desired α-bromomethylketones **10a−c**.[28] Condensation of 2,4-diamino-6-hydroxypyrimidine with **10a−c** afforded the 6-substituted pyrrolo[2,3-*d*]pyrimidines **11a−c**. Optimal yields (38−40%) were obtained at room temperature for 3 days. Trace amounts of two side products were also obtained. No corresponding 5-substituted furo[2,3-*d*]pyrimidines **11d** were obtained in this reaction compared with the condensation of α-chloromethylketones with the pyrimidine that afforded both pyrrolo[2,3-*d*]pyrimidines and furo[2,3-*d*]pyrimidines.[22,23] Hydrolysis of **11a−c** afforded the corresponding free acids **12a−c**. Subsequent coupling with diethyl L-glutamate using *N*-methylmorpholine and 2,4-dimethoxy-6-chlorotriazine as the activating agents[29] (modification from isobutylchloroformate and triethylamine used in the previous report[22,23] for **2** and **3**) afforded the diesters **13a−c**. Final saponification of the diesters gave the target compounds **3−5**.

Biological Evaluation and Discussion

Characterization of 6-Substituted Pyrrolo[2,3-*d*]pyrimidine Antifolates as Substrates for Cellular Uptake by FRs but Not RFC. Isogenic CHO cell line models were developed to easily discriminate antifolate agents accumulated within cells by FRs but not by RFC. We used RFC-null and FR-null MTXRII-Oua^{R}2-4 (R2) CHO cells as the parental subline[30] for our

transfections. R2 cells were transfected with human RFC cDNA to generate a cell line, PC43-10, that expressed high levels of human RFC,[31] accompanying restored transport of [³H]MTX (Figure 2). R2 sublines were also developed that expressed FRs α and β (designated RT16 and D4, respectively) by transfections with cDNAs for these proteins. FRs were accurately quantitated by binding of [³H]folic acid at 0 °C in the absence and presence of excess (5 μM) unlabeled folic acid. By this assay, FRα levels in RT16 cells were high and similar to those in FRα-overexpressing KB tumor cells and were approximately 5-fold higher than those in IGROV1 tumor cells (Figure 2). As expected, [³H]MTX uptake by FRs was nominal in RT16 and
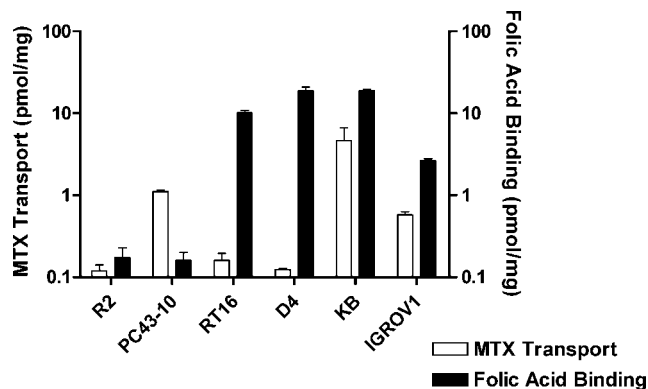

Figure 2. RFC transport and FR binding activities for cell line models. Assorted cell line models including R2, PC43-10, RT16, D4, KB, and IGROV1 were assayed for [³H]MTX uptake as a measure of RFC levels and [³H]folic acid binding as a measure of FR levels. Assays were performed as described in the Experimental Section. For both transport and binding assays, radioactive substrate was expressed in units of pmol/mg protein. FA is folic acid. Results are presented as mean values ± SEM from three experiments.

Table 1. IC$_{50}$ Values (nM) for Compounds **1−5** in Cell Proliferation Inhibition of RFC- and FR-Expressing Cell Lines[a]

| antifolate | hRFC | | hFRα | | hFRβ | | hRFC/FRα | | hRFC/FRα | |
	PC43-10	R2	RT16	RT16 (+folic acid)	D4	D4 (+folic acid)	KB	KB (+folic acid)	IGROV1	IGROV1 (+folic acid)
1	>1000	>1000	>1000	>1000	>1000	>1000	>1000	>1000	>1000	>1000
2	304(89)	448(78)	4.1(1.6)	>1000	5.6(1.2)	>1000	1.7(0.4)	>1000	2.2(0.8)	>1000
3	>1000	>1000	6.3(1.6)	>1000	10(2.0)	>1000	1.9(0.7)	>1000	3.6(0.9)	>1000
4	>1000	>1000	54(21)	>1000	80(9)	>1000	13(7.2)	>1000	40(12)	>1000
5	>1000	>1000	162(18)	>1000	198(34)	>1000	23(12)	>1000	309(77)	>1000
methotrexate	12(1.1)	216(8.7)	114(31)	461(62)	106(11)	211(43)	6.0(0.6)	20(2.4)	21(3.4)	22(2.1)
pemetrexed	138(13)	894(93)	42(9)	388(68)	60(8)	254(78)	68(12)	327(103)	102(25)	200(18)
raltitrexed	6.3(1.3)	>1000	15(5)	>1000	22(10)	746(138)	5.9(2.2)	22(5)	12.6(3.3)	20(4.3)
lometrexol	12(2.3)	>1000	12(8)	188(41)	2.6(1.0)	275(101)	1.2(0.6)	31(7)	3.1(0.9)	16(6)
trimetrexate	25(7.3)	6.7(1.3)	13(1)	4.1(1)	11(4.2)	6.1(1.9)	58(18)	155(38)	12(4)	8.6(1.9)
5a	11(3.3)	>1000	277(81)	>1000	52(12)	>1000	5.8(3.5)	32(15)	5.2(1.7)	6.9(1.6)

[a] Cytotoxicity assays were performed as described in the Experimental Section. For the FR experiments, cytotoxicity assays were performed in the absence and presence of 200 nM folic acid. The data shown are mean values from three experiments (±SEM in parentheses).

D4 cells under standard transport conditions (0.5 μM MTX, 2 min at 37 °C). Thus, the appreciable MTX uptake measured in KB and IGROV1 cells must reflect the expression of RFC in these cells.

The CHO cell lines were initially screened for sensitivities to classical antifolate inhibitors including MTX, PMX, RTX, LMX, and **5a** and to the nonclassical antifolate trimetrexate (TMQ) (structures are shown in Figure 1) by a fluorescence-based cytotoxicity assay. Cells were continuously incubated with drugs for 3−4 days in complete media (includes 2.3 μM folic acid) for R2 and PC43-10 cells or in complete folate-free media supplemented with 2 nM leucovorin [(6R,S)5-formyl tetrahydrofolate] (LCV) (for RT16 and D4 cells). For the FR-expressing sublines, FR-mediated cellular uptake was verified by adding 200 nM folic acid to the incubations. On the basis of its extraordinarily high affinity for FRs, excess folic acid can reverse the growth inhibitory effects of drugs that use this mechanism for cellular entry.[15] PC43-10 cells showed high level sensitivities to all of the classical antifolates, whereas R2 cells were 7- to 150-fold less sensitive to these drugs (Table 1). Collateral sensitivity to TMQ was detected in transport-impaired R2 cells, reflecting its non-RFC mediated uptake and decreased net uptake of cellular folates due to the loss of RFC. For FRα-expressing RT16 cells, LMX showed activity similar to that measured for PC43-10 cells; however, its effects were largely abolished with excess folic acid, confirming FR-mediated uptake. Analogous results were obtained for the FRβ-expressing D4 subline. FRα-expressing KB and IGROV1 human tumor cells showed various sensitivities to classical antifolates and TMQ that were only slightly affected by folic acid, consistent with the presence of both RFC and FR uptake mechanisms in these cells.

The series of 6-substituted pyrrolo[2,3-d]pyrimidine antifolates **1−5** (Figure 1) was screened in the CHO sublines by in vitro drug sensitivity assays as measures of their capacities for cellular uptake by RFC versus FRs (Table 1). Only analogue **2** showed significant (albeit low level) growth inhibitory activity (IC$_{50}$ = 304 nM) toward RFC-expressing PC43-10 cells; however, the level was nearly identical for R2 cells, suggesting the additional involvement of an unidentified non-RFC mechanism of cellular uptake. While the analogue with a one-carbon bridge (compound **1**) was also inactive toward both RT-16 and D4 cells, compounds **2−5** (three- to six-carbon bridge, respectively) showed potent inhibition against the FR-expressing sublines with IC$_{50}$ values in the low to moderate nanomolar range. Analogues **2** and **3** with 3- and 4-methylene groups in the bridge, respectively, were the most potent of this series, and there were no obvious differences in their activities toward

FRα (RT16) versus FRβ (D4) expressing cells. For both RT-16 and D4 cells, the growth inhibitory effects of compounds **2−5** were completely abolished in the presence of excess (200 nM) folic acid, indicating the specific utilization of FRs by these analogues.

Analogous patterns of drug sensitivity and protection by folic acid were seen with KB and IGROV1 human tumor cells (Table 1). In order to assess the effects of increasing levels of extracellular reduced folate on the activity of **3**, KB cells were treated in complete folate-free media including 2−100 nM LCV. As shown in Figure 3A, IC$_{50}$ values increased approximately 3-fold between 2 and 20 nM LCV and up to ∼6-fold at 40 nM LCV.

Thus, the in vitro cytotoxicity results establish that the growth inhibitory effects of compounds **2−5** are dependent on their cellular accumulation via FRs rather than RFC and that there is no apparent difference in the activity of these drugs toward cells that express the FRα isoform from cells that express FRβ. There appears to be a modest antagonistic effect of exogenous reduced folates on antifolate activity of compound **3** over a physiologic range of reduced folate.

Protection from the Growth Inhibitory Effects of 6-Substituted Pyrrolo[2,3-d]pyrimidine Antifolates with Nucleosides To Identify the Cytotoxic Locus. Since the growth inhibitory effects of most antifolates involve enzyme targets leading to nucleotides, thymidine (10 μM) and adenosine (60 μM) were evaluated for their capacities to protect from the growth inhibitory effects of the 6-substituted pyrrolo[2,3-d]pyrimidine antifolates **2−5** toward KB cells. These nucleoside concentrations are capable of completely reversing the cytotoxic effects of classical antifolates such as MTX (requires both thymidine and adenosine), LMX (requires adenosine), and PMX (typically requires only thymidine, although adenosine may be required at higher drug concentrations) (not shown).

Whereas 10 μM thymidine had no effect on the activity of **2** toward KB cells (thus eliminating TS as an important drug target), growth inhibition was completely reversed in the presence of 60 μM adenosine [Figure 3B shows results with compound **2**; identical results were obtained with compounds **3−5** (data not shown)]. Analogous results were also obtained with RT16, D4, and IGROV1 cells (data not shown). Since de novo purine biosynthesis involves two folate-dependent steps [catalyzed by GARFTase and 5-amino-4-imidazole carboxamide ribonucleotide formyltransferase (AICARFTase)], additional protection experiments were performed with 5-amino-4-imidazole carboxamide (AICA), a precursor of the purine biosynthetic intermediate 5-amino-4-imidazolecarboxamide ribonucleotide (AICAR), which circumvents the step catalyzed by GARFTase
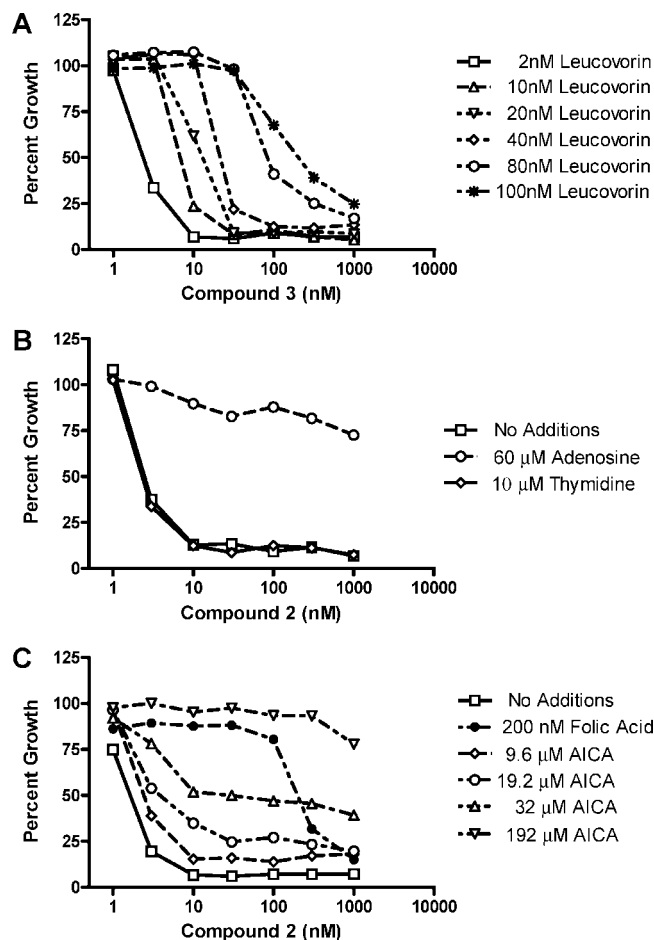
Figure 3. Cell proliferation inhibition and protection by nucleosides and folates. Cell proliferation inhibition was measured on 96-well plates with 4000 KB cells per well initially and a range of antifolate concentrations (1−1000 nM) in the presence or absence of the following: LCV (2−100 nM) (A); adenosine (60 μM) or thymidine (10 μM) (B); folic acid (200 nM) or AICA (9.6−192 μM) (C). Cell densities were measured with CellTiter Blue fluorescence dye and a fluorescence plate reader. Results were normalized to cell density in the absence of drug. Results shown are representative data of experiments performed in triplicate.

(Figure 4). As shown in Figure 3C, KB cells were completely protected by 192 μM AICA from the growth inhibitory effects of **2**, whereas lower AICA concentrations were less effective. Identical results were obtained with RT16, D4, and IGROV1 cells (not shown). Likewise, AICA was completely protective of the growth inhibitory effects of compounds **3−5** (not shown).

Inhibitory Effects of 6-Substituted Pyrrolo[2,3-*d*]pyrimidine Antifolates on RFC Transport and FR Binding. Although the cytotoxicity data in the CHO sublines (Table 1) strongly implied that cellular uptake of the 6-substituted pyrrolo[2,3-*d*]pyrimidine antifolates was by FRs (both α and β) rather than RFC, additional studies were performed to directly address this question.

For this series of experiments, the PC43-10 CHO subline ectopically expressing wild type RFC[31] was used to determine the inhibitory effects of analogues **1−5** on RFC-mediated [³H]MTX uptake as a measure of their substrate activities. Although PMX, MTX, LMX, and LCV (each at 10 μM) were all potently inhibitory (60−70%) to [³H]MTX uptake, folic acid and compounds **1−5** were only slightly inhibitory (<20%; Figure 5A). This strongly suggests that the 6-substituted

pyrrolo[2,3-*d*]pyrimidine antifolates **1−5** are poor RFC substrates, consistent with the in vitro cytotoxicity results (Table 1).

Additional experiments were performed to test the relative binding affinities for FRα and FRβ for compounds **1−5**, compared to those for folic acid (Figure 5B). MTX, PMX, LMX and LCV were also tested. For these determinations, RT16 (FRα) and D4 (FRβ) cells were incubated in 50 nM [³H]folic acid in the presence of a range of inhibitor concentrations. Using relative binding of folic acid set to a value of 1, both compound **1** and MTX bound poorly (relative binding <0.01) (Figure 5A). LMX showed high and comparable affinities for FRα and FRβ; however, lower and disparate affinities were detected for PMX and LCV for FRα and FRβ. Similar results were previously reported for LCV.[10] When binding affinities for compounds **2−5** were measured, **3−5** all showed similarly high affinities that were only slightly increased from those for **2** (Figure 5B). These results further establish that compounds **2−5** are all excellent substrates for both α and β forms of FR.

Validation of GARFTase as the Primary Intracellular Target for 6-Substituted Pyrrolo[2,3-*d*]pyrimidine Antifolates. The protection experiments with AICA (Figure 3) strongly suggested GARFTase as the probable major intracellular target for the 6-substituted pyrrolo[2,3-*d*]pyrimidine antifolates **2−5**. GARFTase catalyzes the formylation of the glycine-derived nitrogen of β-glycinamide ribonucleotide (βGAR) using 10-formyl tetrahydrofolate as one carbon donor (Figure 4). GARFTase has been identified as a primary target for LMX[32] and as a secondary target after TS for PMX.[33] To establish inhibition of GARFTase for compounds **2−5**, two approaches were used and the results were compared to those for PMX and LMX.

In vitro enzyme inhibitory effects were directly assessed over a range of antifolate concentrations (10−30000 nM) toward purified recombinant mouse GARFTase, by following the spectral change at 285.5 nm accompanying one-carbon transfer from 10-formyl-5,8-dideazafolic acid to GAR, forming 5,8-dideazafolic acid and formyl GAR. IC$_{50}$ values are summarized in Table 2 and ranged from 0.15 μM for compound **3** to 2.5 μM for compound **5**. Thus, analogue **3** with the four-atom bridge is the most potent inhibitor of GARFTase, whereas inhibitions by the three-, five-, and six-carbon analogues were approximately 16-fold lower and nearly identical. Compound **3** was approximately 5-fold more potent than LMX and more than 134-fold more potent than PMX toward recombinant mouse GARFTase.

To complement the isolated enzyme studies, additional experiments were performed to measure in situ inhibition of GARFTase in KB cells, as measured by [¹⁴C]glycine incorporation into [¹⁴C]formyl GAR in the presence of azaserine.[32] For this assay, KB cells were incubated for 18 h with and without the antifolates (over a range of concentrations) in the presence of 10 μM azaserine. Cells were washed with PBS, proteins were precipitated, the supernatants were extracted with ether, and the aqueous layer was fractionated on columns of AG1X-10 (Cl⁻) (Figure 6, left panel). Inhibitions of [¹⁴C]formyl GAR synthesis in KB cells for compounds **2** and **3** are shown in Figure 6 (right panel). IC$_{50}$ values for the in situ GARFTase assays for all the antifolates are summarized in Table 2 and clearly demonstrate that treatments with compounds **2−5** potently inhibit [¹⁴C]glycine incorporation into [¹⁴C]formyl GAR at nanomolar concentrations approaching those in the proliferation assays (Table 1).

Collectively, these experiments establish that the 6-substituted pyrrolo[2,3-*d*]pyrimidine series are bona fide inhibitors of
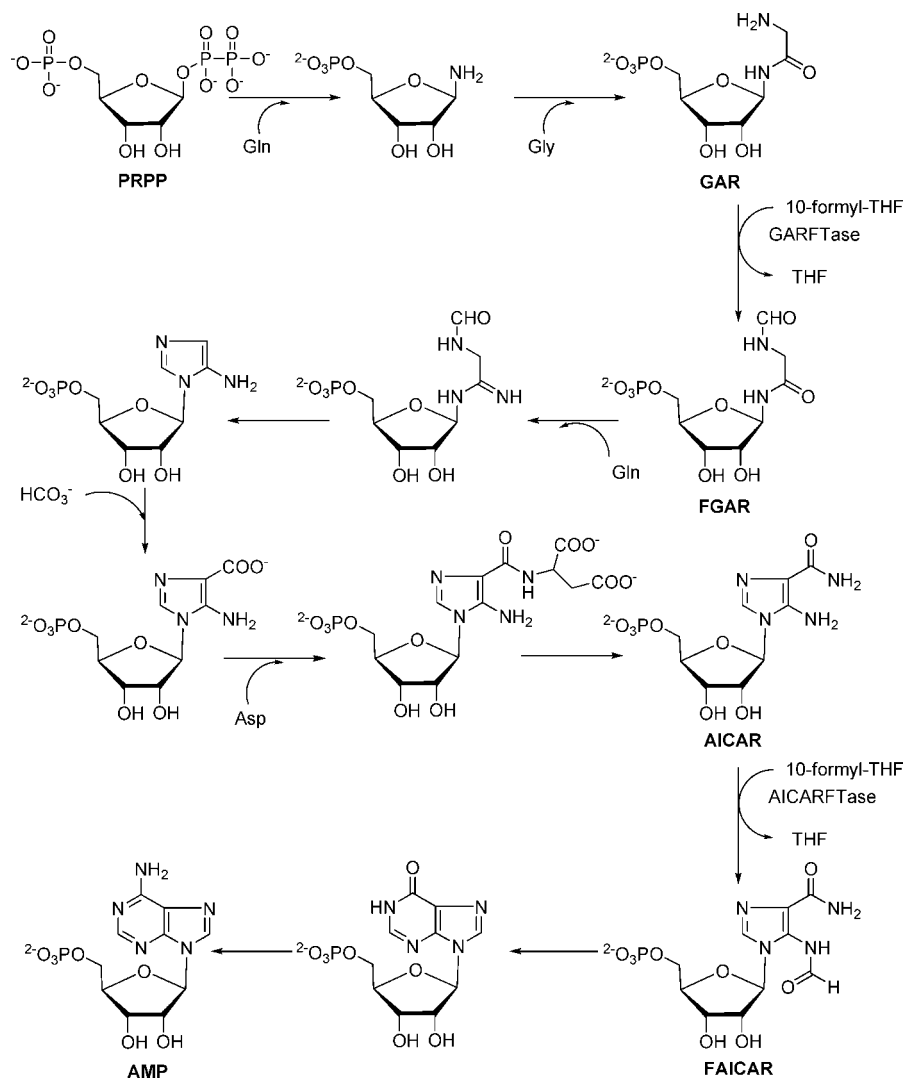
Figure 4. De novo purine nucleotide biosynthesis pathway. The de novo purine nucleotide biosynthetic pathway from phosphoribosyl pyrophosphate (PRPP) to AMP is shown. There are two folate-dependent reactions in which 10-formyl tetrahydrofolate serves as the one carbon donor: GARFTase and AICAR formyltransferase. AICA can be metabolized to AICAR, thus circumventing the reaction catalyzed by GARFTase. For the in situ GARFTase assay, incorporation of [14C]glycine into formyl GAR (FGAR) in the presence of azaserine is used as a direct measure of GARFTase activity.

GARFTase, in direct support of the results from the AICA cytotoxicity protection experiments. The disparity in relative inhibitory concentrations for cell growth and in situ GARFTase versus those for the purified GARFTase likely reflects the synthesis of antifolate polyglutamates within cells and greater inhibitory potency of polyglutamate over monoglutamate antifolates toward GARFTase, analogous to LMX.[24] Consistent with this notion, analogues **2** and **3** were previously reported to be excellent substrates for polyglutamylation by human folylpolyglutamate synthetase.[23]

Effects of 6-Substituted Pyrrolo[2,3-d]pyrimidine Antifolates on Colony Formation and Apoptosis. While antipurine antifolates such as LMX were suggested to be cytostatic rather than cytotoxic,[34] in another report LMX was distinctly cytotoxic[35] although not necessarily apoptotic. Interestingly, for TS-targeted therapies, necrosis rather than apoptosis was reported as the primary mechanism of cell killing.[36] To shed light on this question for the pyrrolo[2,3-d]pyrimidine GARFTase inhibitors, two approaches were used, including (i) assays of colony formation and reversibility and (ii) apoptosis assays by annexin-PI staining.

By colony forming assay with KB cells, compounds **2** and **3** were more potent inhibitors than either compound **4** or MTX (Figure 7A), analogous to the results for growth inhibition assays with these compounds (Table 1). To assess reversibility of antifolate effects, cells were treated with 1 μM compound **3** for 48 h, then washed, counted, and replated into drug-free medium. Colonies were enumerated after 14 days, and the results were compared to those for untreated cells and for cells treated on an identical schedule with 1 μM of classical antifolate inhibitors (MTX, PMX, RTX, and LMX). Even in the absence of continuous drug treatments, all of the agents were potent inhibitors of colony formation (Figure 7B) with relative inhibitions ranging from >97% for compound **3** to >99% for RTX.

To assay apoptosis, KB cells were treated for 24 h with classical antifolates (PMX, RTX, or LMX) or with compound **3** (all at 1 μM). Cells were treated with daunorubicin (1 μM) as a positive control. Cells were stained with annexin V-FITC, and annexin V positive cells were measured by flow cytometry. In triplicate experiments, daunorubicin induced a high level of apoptosis, exceeding that resulting from any of the antifolate drugs by a factor of 4 (Figure 8). These results strongly suggest
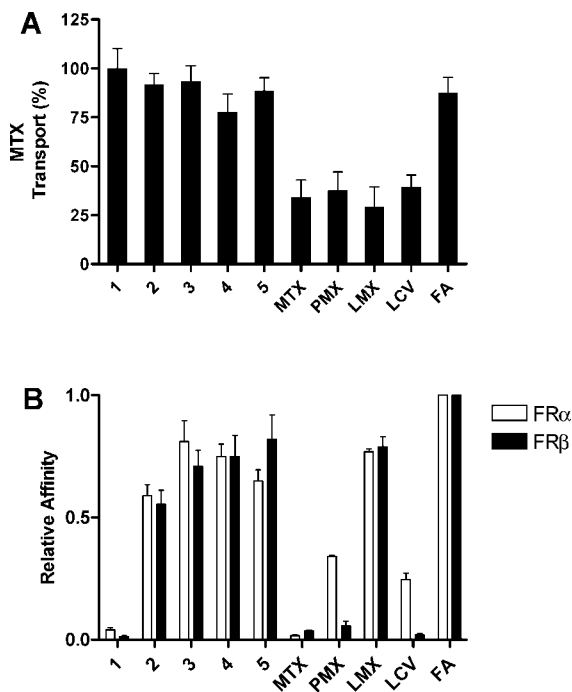
Figure 5. Competitive inhibition of RFC transport and FR binding activities by 6-substituted pyrrolopyrimidines. (A) PC43-10 cells ectopically expressing wild type RFC but no FR[31] were assayed for [³H]MTX in the presence of the pyrrolopyrimidine antifolates **1–5**, MTX, PMX, LMX, LCV, or folic acid (each at 10 μM). (B) Data are shown for the effects of the unlabeled ligands with FRα-expressing RT16 CHO cells and FRβ-expressing D4 CHO cells. Relative binding affinities for assorted folate/antifolate substrates were determined over a range of ligand concentrations and were calculated as the inverse molar ratio of unlabeled ligands required to inhibit [³H]folic acid binding by 50%. By definition, the relative affinity of folic acid is 1. Details for the transport and binding assays are provided in the Experimental Section. Abbreviations are as follows: MTX, methotrexate; PMX, pemetrexed; LMX, lometrexol; LCV, leucovorin; FA, folic acid. Results are presented as mean values ± SEM from three experiments.

Table 2. IC$_{50}$ Values for Pyrrolopyrimidine Compounds **1–5** in in Vitro and in Situ GARFTase Inhibition Assays[a]

	IC$_{50}$	
antifolate	in vitro (μM)	in situ (nM)
1	>20	>1000
2	2.44 (0.12)	18(2.0)
3	0.15 (0.01)	6.8(0.9)
4	2.26 (0.16)	7.2(1.8)
5	2.51 (0.25)	8.6(0.7)
pemetrexed	>20	30(7.7)
lometrexol	0.78 (0.08)	14(5.6)

[a] GARFTase inhibition assays, both in vitro and in situ, were performed as described in the Experimental Section. The IC$_{50}$ data shown are mean values from three (in vitro, SEM in parentheses) or two (in situ, range in parentheses) experiments.

that cell death resulting from either inhibition of TS or GARFTase in KB cells is not predominantly apoptotic.

Thus, the effects of the 6-substituted pyrrolo[2,3-*d*]pyrimidine antifolates on clonogenicity and cell proliferation were both profound and largely irreversible. Cell killing, however, was largely independent of apoptosis.

In summary, we have described for the first time the specific FR targeting ability of a series of 6-subsituted pyrrolo[2,3-*d*]pyrimidine antifolates **2–5** that irreversibly inhibit cell proliferation and colony formation by potently suppressing de novo purine nucleotide biosynthesis at the level of GARFTase.

We have identified distinct structure–activity relationships for this series involving the length of the methylene "bridge" region between the pyrrolo[2,3-*d*]pyrimidine and the *p*-aminobenzoyl-L-glutamate, with increased FR binding for compounds **2–5** (three to six methylenes) over compound **1** (one methylene group) and optimal inhibition of GARFTase by compound **3** (four methylenes). The complete lack of detectable RFC transport for these analogues and antiproliferative effects even in the presence of physiologic concentrations of reduced folates suggests their potential for selectively targeting tumors that express FRs. The combined properties of selective FR targeting, lack of RFC transport, and GARFTase inhibition resulting in potent antitumor activity are unprecedented and certainly warrant further study including in vivo antitumor activities and the synthesis of additional analogues to optimize cellular uptake by FRs and inhibition of GARFTase. These studies are currently underway and will be the subject of future reports.

Experimental Section

All evaporations were carried out in vacuo with a rotary evaporator. Analytical samples were dried in vacuo (0.2 mmHg) in a CHEM-DRY drying apparatus over P$_2$O$_5$ at 80 °C. Melting points were determined on a MEL-TEMP II melting point apparatus with FLUKE 51 K/J electronic thermometer and are uncorrected. Nuclear magnetic resonance spectra for proton (¹H NMR) were recorded on a Bruker WH-300 (300 MHz) or a Bruker 400 MHz/ 52 MM (400 MHz) spectrometer. The chemical shift values are expressed in ppm (parts per million) relative to tetramethylsilane as internal standard: s, singlet; d, doublet; t, triplet; q, quartet; m, mutiplet; br, broad singlet. The relative integrals of peak areas agreed with those expected for the assigned structures. High-resolution mass spectra (HRMS), using electron impact (EI), were recorded on a VG AUTOSPEC (Fisons Instruments) micromass (EBE Geometry) double focusing mass spectrometer. Thin-layer chromatography (TLC) was performed on Whatman Sil G/UV254 silica gel plates with fluorescent indicator, and the spots were visualized under 254 and 366 nm illumination. Proportions of solvents used for TLC are by volume. Column chromatography was performed on 230–400 mesh silica gel purchased from Aldrich, Milwaukee, WI. Elemental analyses were performed by Atlantic Microlab, Inc., Norcross, GA. Element compositions are within ±0.4% of the calculated values. Fractional moles of water or organic solvents frequently found in some analytical samples of antifolates could not be prevented despite 24–48 h of drying in vacuo and were confirmed where possible by their presence in the ¹H NMR spectra. All solvents and chemicals were purchased from Aldrich Chemical Co. or from Fisher Scientific and were used as received.

(4*E/Z*)-5-[4-(Methoxycarbonyl)phenyl]pent-4-enoic Acid (8a). Compound **8a** was synthesized as reported previously:[23] yield 94% as white crystals, mp 121–123 °C (lit.[23] mp 118–121 °C), R$_f$ = 0.20 (hexane/EtOAc, 3:1). ¹H NMR (DMSO-d$_6$) δ 2.40–2.46 (m, 4 H, 2 CH$_2$), 3.84 (s, 3 H, OCH$_3$), 6.47–6.52 (m, 2 H, CH=CH), 7.52 (d, 2 H, C$_6$H$_4$, *J* = 4.1 Hz), 7.89 (d, 2 H, C$_6$H$_4$, *J* = 4.2 Hz), 12.18 (br, 1H, COOH).

(5*E/Z*)-6-[4-(Methoxycarbonyl)phenyl]hex-5-enoic Acid (8b). Compound **8b** was synthesized as described for **8a**: yield 90% as white crystals, mp 77–81 °C, R$_f$ = 0.22 (hexane/EtOAc, 3:1). ¹H NMR (DMSO-d$_6$) δ 1.60–1.76 (m, 2 H, CH$_2$), 2.20–2.35 (m, 4 H, 2 CH$_2$), 3.84(s, 3 H, OCH$_3$), 6.45–6.55 (m, 2 H, CH=CH), 7.53 (d, 2 H, C$_6$H$_4$, *J* = 4.0 Hz), 7.89 (d, 2 H, C$_6$H$_4$, *J* = 4.0 Hz), 12.06 (br, 1H, COOH). Anal. (C$_{14}$H$_{16}$O$_4$) C, H.

(6*E/Z*)-7-[4-(Methoxycarbonyl)phenyl]hept-6-enoic Acid (8c). Compound **8c** was synthesized as described for **8a**: yield 92% as white crystals, mp 72–73 °C, R$_f$ = 0.26 (hexane/EtOAc, 3:1). ¹H NMR (CDCl$_3$) δ 1.48–1.76 (m, 4 H, 2 CH$_2$), 2.23–2.44 (m, 4 H, 2 CH$_2$), 3.91 (s, 3 H, OCH$_3$), 6.30–6.50 (m, 2 H, CH=CH), 7.32 (d, 2 H, C$_6$H$_4$, *J* = 4.0 Hz), 7.97 (d, 2 H, C$_6$H$_4$, *J* = 4.0 Hz). Anal. (C$_{15}$H$_{18}$O$_4$) C, H.
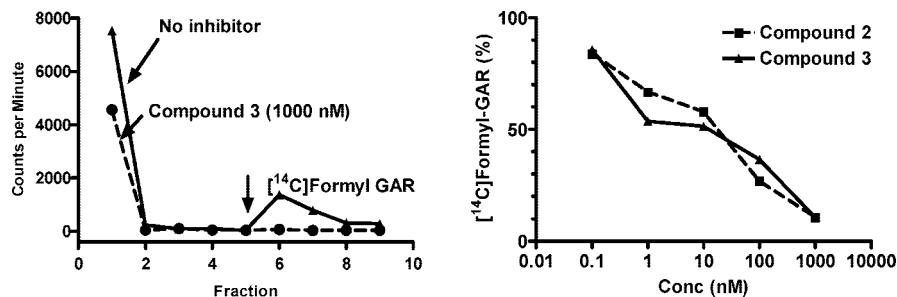
Figure 6. GARFTase inhibition by 6-substituted pyrrolopyrimidine antifolates in situ. GARFTase activity and inhibition were evaluated in situ with KB cells. For these experiments, KB cells were treated with [14C]glycine in presence or absence of 4 μM azaserine. After 15 h, radioactive metabolites were extracted and fractionated on 1 cm columns of AG1x8(Cl$^-$) and the fractions were collected and determined for radioactivity. Accumulation of [14C]formyl GAR (FGAR) was calculated as pmol/mg protein over a range of antifolate concentrations. In the left panel, an elution profile for a typical elution for cells untreated and treated with 1000 nM compound **3** is shown. The arrow designates 1 N HCl elution of [14C]formyl GAR. In the right panel are shown the data for the percent inhibition of in situ activity over a range of compound **3** concentrations as described in the text. Data summarizing inhibitions of in situ GARFTase activity are summarized in Table 2.
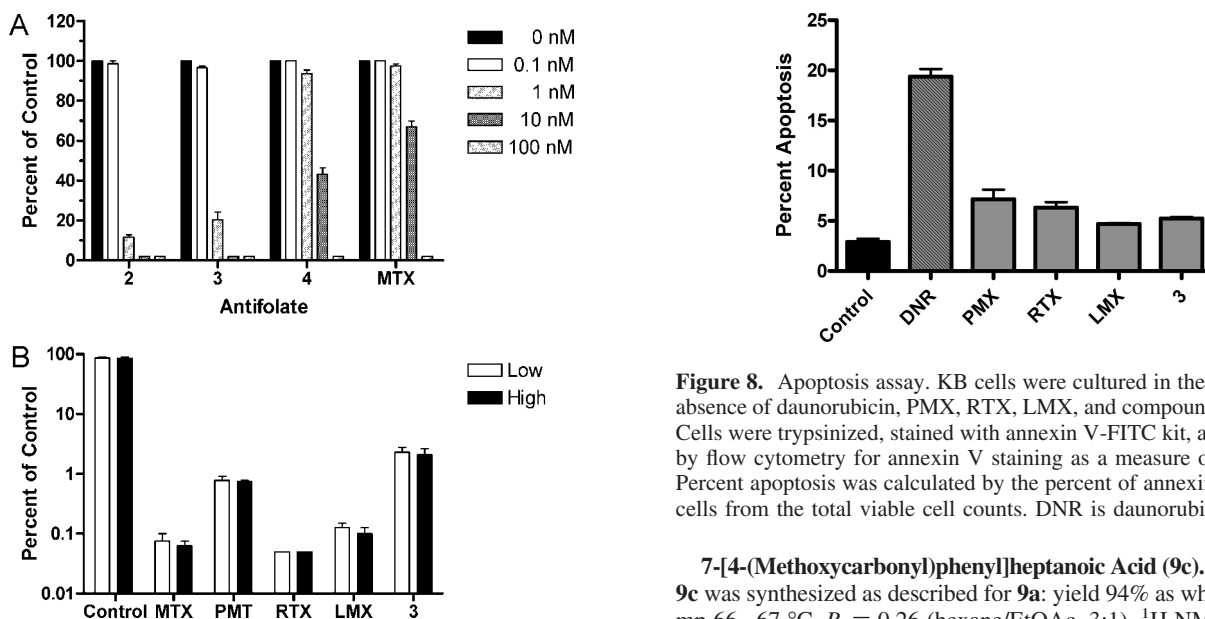

Figure 7. Colony-forming inhibition assay. (A) KB cells were plated into 60 mm dishes with a density of 100 cells per dish in the presence or absence of different concentrations of drugs from 0.1 to 100 nM. Colonies were enumerated after 10 days. Data were calculated as percent of controls treated identically but without drugs. (B) KB cells were cultured in the presence or absence of 1 μM antifolate compounds for 2 days. Cells were washed with saline, trypsinized, and replated into 60 mm dishes at low and high densities (200 and 400, or 2000 and 4000 cells per dish for cells cultured in the absence or presence of antifolate, respectively). Colonies were counted after 14 days, and colony-forming efficiencies were calculated for each compound. Results are presented as mean values from three experiments ($\pm$SEM for part A) or from two experiments ($\pm$range for part B).

5-[4-(Methoxycarbonyl)phenyl]pentanoic Acid (9a). Compound **9a** was synthesized as reported previously:[23] yield 100% as white crystals, mp 85–86 °C (lit.[23] mp 86.9–88.5 °C), R_f = 0.25 (hexane/EtOAc, 3:1). ^{1}H NMR (DMSO-d_6) δ 1.40–1.70 (m, 4 H, 2 CH$_2$), 2.23 (t, 2 H, CH$_2$), 2.66 (t, 2 H, CH$_2$), 3.83 (s, 3 H, OCH$_3$), 7.34 (d, 2 H, C$_6$H$_4$, J = 3.9 Hz), 7.88 (d, 2 H, C$_6$H$_4$, J = 3.9 Hz), 12.04 (s, 1H, COOH).

6-[4-(Methoxycarbonyl)phenyl]hexanoic Acid (9b). Compound **9b** was synthesized as described for **9a**: yield 99% as white crystals, mp 49–51 °C, R_f = 0.26 (hexane/EtOAc, 3:1). ^{1}H NMR (CDCl$_3$) δ 1.34–1.43 (m, 2 H, CH$_2$), 1.58–1.72 (m, 4 H, 2 CH$_2$), 2.35 (t, 2 H, CH$_2$), 2.66 (t, 2 H, CH$_2$), 3.89 (s, 3H, OCH$_3$), 7.23 (d, 2 H, C$_6$H$_4$, J = 4.0 Hz), 7.94 (d, 2 H, C$_6$H$_4$, J = 4.0 Hz). Anal. (C$_{14}$H$_{18}$O$_4$) C, H.

Figure 8. Apoptosis assay. KB cells were cultured in the presence or absence of daunorubicin, PMX, RTX, LMX, and compound **3** for 24 h. Cells were trypsinized, stained with annexin V-FITC kit, and analyzed by flow cytometry for annexin V staining as a measure of apoptosis. Percent apoptosis was calculated by the percent of annexin V positive cells from the total viable cell counts. DNR is daunorubicin.

7-[4-(Methoxycarbonyl)phenyl]heptanoic Acid (9c). Compound **9c** was synthesized as described for **9a**: yield 94% as white crystals, mp 66–67 °C, R_f = 0.26 (hexane/EtOAc, 3:1). ^{1}H NMR (CDCl$_3$) δ 1.27–1.42 (m, 4 H, 2 CH$_2$), 1.50–1.71 (m, 4 H, 2 CH$_2$), 2.33 (t, 2 H, CH$_2$), 2.64 (t, 2 H, CH$_2$), 3.89 (s, 3H, OCH$_3$), 7.20 (d, 2 H, C$_6$H$_4$, J = 4.0 Hz), 7.94 (d, 2 H, C$_6$H$_4$, J = 4.0 Hz). Anal. (C$_{15}$H$_{20}$O$_4$·0.1CH$_3$COOC$_2$H$_5$) C, H.

Methyl 4-(6-Bromo-5-oxohexyl)benzoate (10a). To a solution of 5-[4-(methoxycarbonyl)phenyl]pentanoic acid (**9a**) (0.36 g, 1.5 mmol) in a 50 mL flask were added oxalyl chloride (1.5 mL) and anhydrous CH$_2$Cl$_2$ (10 mL). The resulting solution was refluxed for 1 h and then cooled to room temperature. After evaporation of solvent under reduced pressure, the residue was dissolved in ethyl ether (20 mL). The resulting solution was added dropwise to an ice-cooled ether solution of diazomethane (generated in situ from 1.4 g N-nitroso-N-methylurea) over 10 min. To this solution was added 48% HBr (1.5 mL). The resulting mixture was refluxed for 1.5 h. After the mixture was cooled to room temperature, the organic layer was separated and the aqueous layer was extracted with ethyl ether (20 mL × 3). The combined organic layers were washed with two portions of 10% Na$_2$CO$_3$ solution and dried over Na$_2$SO$_4$. The solvent was evaporated to afford 0.44 g (90%) of **10a** as yellow needles: mp 65–66 °C, R_f = 0.45 (hexane/EtOAc, 3:1). ^{1}H NMR (DMSO-d_6) δ 1.43–1.65 (m, 4 H, 2 CH$_2$), 2.54–2.74 (m, 4 H, 2 CH$_2$), 3.83 (s, 3 H, OCH$_3$), 4.32 (s, 2H, CH$_2$Br), 7.34 (d, 2 H, C$_6$H$_4$, J = 4.0 Hz), 7.87 (d, 2 H, C$_6$H$_4$, J = 4.0 Hz).

Methyl 4-(7-Bromo-6-oxoheptyl)benzoate (10b). Compound **10b** was synthesized as described for **10a**: yield 80% as white crystals, mp 55–56 °C, R_f = 0.52 (hexane/EtOAc, 3:1). ^{1}H NMR (CDCl$_3$) δ 1.30–1.42 (m, 2 H, CH$_2$), 1.59–1.72 (m, 4 H, 2 CH$_2$), 2.61–2.70 (m, 4 H, 2 CH$_2$), 3.87 (s, 2H, CH$_2$Br), 3.90 (s, 3 H, OCH$_3$), 7.23

(d, 2 H, C₆H₄, *J* = 4.0 Hz), 7.95 (d, 2 H, C₆H₄, *J* = 4.0 Hz). HRMS calcd for C₁₅H₁₉BrO₃ 326.0518, found 326.0524.

Methyl 4-(8-Bromo-7-oxooctyl)benzoate (10c). Compound **10c** was synthesized as described for **10a**: yield 85% as yellow crystals, mp 47−48 °C, R_f = 0.53 (hexane/EtOAc, 3:1). ¹H NMR (CDCl₃) δ 1.30−1.39 (m, 4 H, 2 CH₂), 1.60−1.71 (m, 4 H, 2 CH₂), 2.58−2.69 (m, 4 H, 2 CH₂), 3.87 (s, 2H, CH₂Br), 3.90 (s, 3 H, OCH₃), 7.23 (d, 2 H, C₆H₄, *J* = 4.0 Hz), 7.95 (d, 2 H, C₆H₄, *J* = 4.0 Hz). HRMS calcd for C₁₆H₂₁BrO₃ 340.0674, found 340.0683.

Methyl 4-[4-(2-Amino-4-oxo-4,7-dihydro-3*H*-pyrrolo[2,3-*d*]pyrimidin-6-yl)butyl]benzoate (11a). To a suspension of 2,4-diamino-6-hydroxypyrimidine (1.53 g, 12.2 mmol) in anhydrous DMF (40 mL) was added **10a** (3.82 g, 12.2 mmol). The resulting mixture was stirred under N₂ at room temperature for 3 days. TLC showed the disappearance of starting materials and the formation of one major spot at R_f = 0.28 (CHCl₃/MeOH, 6:1). After evaporation of solvent, CH₃OH (20 mL) was added followed by silica gel (5 g). Evaporation of the solvent afforded a plug, which was loaded onto a silica gel column (3.5 cm × 15 cm) and eluted initially with CHCl₃ followed by 10% MeOH in CHCl₃ and then 15% MeOH in CHCl₃. Fractions showing R_f = 0.28 were pooled and evaporated, and the resulting solid was recrystallized from MeOH to afford 1.53 g (37%) of **11a** as yellow crystals: mp 240−241 °C (lit.[23] mp 241.9−243.7 °C). This compound was identical in all respects to that reported in the literature.[23] ¹H NMR (DMSO-*d₆*) δ 1.52−1.62 (m, 4 H, 2 CH₂), 2.49−2.71 (m, 4 H, 2 CH₂), 3.83 (s, 3 H, OCH₃), 5.84 (s, 1 H, CH), 5.95 (s, 2 H, 2-NH₂), 7.34 (d, 2 H, C₆H₄, *J* = 4.0 Hz), 7.87 (d, 2 H, C₆H₄, *J* = 4.0 Hz) 10.12 (s, 1 H, 3-NH), 10.80 (s, 1H, 7-NH).

Methyl 4-[5-(2-Amino-4-oxo-4,7-dihydro-3*H*-pyrrolo[2,3-*d*]pyrimidin-6-yl)pentyl]benzoate (11b). Compound **11b** was synthesized as described for **11a**: yield 35% as yellow crystals, mp 229−230 °C, R_f = 0.31 (CHCl₃/MeOH, 6:1). ¹H NMR (DMSO-*d₆*) δ 1.26−1.36 (m, 2 H, CH₂), 1.52−1.66 (m, 4 H, 2 CH₂), 2.48−2.68 (m, 4 H, 2 CH₂), 3.82 (s, 3 H, OCH₃), 5.84 (s, 1 H, CH), 5.95 (s, 2 H, 2-NH₂), 7.33 (d, 2 H, C₆H₄, *J* = 4.0 Hz), 7.86 (d, 2 H, C₆H₄, *J* = 4.0 Hz) 10.12 (s, 1 H, 3-NH), 10.79 (s, 1H, 7-NH). Anal. (C₁₉H₂₂N₄O₃·0.2H₂O) C, H, N.

Methyl 4-[6-(2-Amino-4-oxo-4,7-dihydro-3*H*-pyrrolo[2,3-*d*]pyrimidin-6-yl)hexyl]benzoate (11c). Compound **11c** was synthesized as described for **11a**: yield 35% as yellow crystals, mp 219−221 °C, R_f = 0.35 (CHCl₃/MeOH, 6:1). ¹H NMR (DMSO-*d₆*) δ 1.25−1.35 (m, 4 H, 2 CH₂), 1.47−1.65 (m, 4 H, 2 CH₂), 2.49−2.67 (m, 4 H, 2 CH₂), 3.82 (s, 3 H, OCH₃), 5.83 (s, 1 H, CH), 5.95 (s, 2 H, 2-NH₂), 7.33 (d, 2 H, C₆H₄, *J* = 4.0 Hz), 7.86 (d, 2 H, C₆H₄, *J* = 4.0 Hz) 10.11 (s, 1 H, 3-NH), 10.76 (s, 1H, 7-NH). Anal. (C₂₀H₂₄N₄O₃·0.67H₂O) C, H, N.

4-[4-(2-Amino-4-oxo-4,7-dihydro-3*H*-pyrrolo[2,3-*d*]pyrimidin-6-yl)butyl]benzoic Acid (12a). To a suspension of **11a** (178 mg, 0.5 mmol) in 10 mL of CH₃OH was added 3 N NaOH (10 mL). The resulting mixture was stirred under N₂ at 40−50 °C for 24 h. TLC indicated the disappearance of starting material and the formation of one major spot at the origin. The resulting solution was passed through Celite and washed with a minimum amount of CH₃OH. The combined filtrate was evaporated under reduced pressure to dryness. To this residue was added distilled water (10 mL). The solution was cooled in an ice bath, and the pH was adjusted to 3−4 using 3 N HCl. The resulting suspension was chilled in a dry ice/acetone bath and thawed to 4 °C overnight in a refrigerator. The precipitate was filtered, washed with cold water, and dried in a desiccator under reduced pressure using P₂O₅ to afford 120 mg (74%) of **12a** as a brown powder: mp >262 °C (dec) (lit.[23] mp >266 °C), R_f = 0.20 (CHCl₃/MeOH, 5:1). This compound was identical in all respects to that reported in the literature.[23]

4-[5-(2-Amino-4-oxo-4,7-dihydro-3*H*-pyrrolo[2,3-*d*]pyrimidin-6-yl)pentyl]benzoic Acid (12b). Compound **12b** was synthesized as described for **12a**: yield 90% as a brown powder, mp >271 °C (dec), R_f = 0.18 (CHCl₃/MeOH, 5:1). ¹H NMR (DMSO-*d₆*) δ 1.26−1.36 (m, 2 H, CH₂), 1.55−1.67 (m, 4 H, 2 CH₂), 2.48−2.69 (m, 4 H, 2 CH₂), 5.85 (s, 1 H, CH), 5.96 (s, 2 H, 2-NH₂), 7.31 (d,

2 H, C₆H₄, *J* = 4.0 Hz), 7.84 (d, 2 H, C₆H₄, *J* = 4.0 Hz), 10.12 (s, 1 H, 3-NH), 10.80 (s, 1H, 7-NH). Anal. (C₁₈H₂₀N₄O₃·0.75CH₃OH) C, H, N.

4-[6-(2-Amino-4-oxo-4,7-dihydro-3*H*-pyrrolo[2,3-*d*]pyrimidin-6-yl)hexyl]benzoic Acid (12c). Compound **12c** was synthesized as described for **12a**: yield 98% as a brown powder, mp >276 °C (dec), R_f = 0.18 (CHCl₃/MeOH, 5:1). ¹H NMR (DMSO-*d₆*) δ 1.24−1.35 (m, 4 H, 2 CH₂), 1.48−1.64 (m, 4 H, 2 CH₂), 2.49−2.66 (m, 4 H, 2 CH₂), 5.84 (s, 1 H, CH), 5.97 (s, 2 H, 2-NH₂), 7.29 (d, 2 H, C₆H₄, *J* = 4.0 Hz), 7.84 (d, 2 H, C₆H₄, *J* = 4.0 Hz), 10.13 (s, 1 H, 3-NH), 10.77 (s, 1H, 7-NH). Anal. (C₁₉H₂₂N₄O₃·1.4H₂O) C, H, N.

Diethyl *N*-{4-[4-(2-Amino-4-oxo-4,7-dihydro-3*H*-pyrrolo[2,3-*d*]pyrimidin-6-yl)butyl]benzoyl}-L-glutamate (13). To a solution of **12a** (290 mg, 0.89 mmol) in anhydrous DMF (40 mL) was added 6-chloro-2,4-dimethoxy-1,3,5-triazine (180 mg, 1.07 mmol) and *N*-methylmorpholine (105 mg, 1.07 mmol). After the mixture was stirred at room temperature for 2 h, *N*-methylmorpholine (105 mg, 1.07 mmol) and dimethyl L-glutamate hydrochloride (423 mg, 1.78 mmol) were added all at once. The mixture was stirred at room temperature for 4 h. TLC showed the formation of one major spot at R_f = 0.55 (CHCl₃/MeOH, 5:1). The reaction mixture was evaporated to dryness under reduced pressure. The residue was dissolved in a minimum amount of CHCl₃/MeOH, 5:1, and chromatographed on a silica gel column (2 cm × 15 cm) with 4% MeOH in CHCl₃ as the eluent. Fractions that showed the desired single spot at R_f = 0.55 were pooled and evaporated to dryness to afford **13a**, 307 mg, yield 68% as a yellow syrup, which was used directly for the next step. ¹H NMR (DMSO-*d₆*) δ 1.08−1.28 (m, 6 H, 2 CH₃), 1.52−1.68 (m, 4 H, 2 CH₂), 1.88−2.15 (m, 2 H, CH₂), 2.40−2.68 (m, 6 H, 3 CH₂), 3.98−4.12 (m, 4 H, 2 CH₂), 4.36−4.46 (m, 1 H, CH), 5.84 (s, 1 H, CH), 5.94 (s, 2 H, 2-NH₂), 7.28 (d, 2 H, C₆H₄, *J* = 4.0 Hz), 7.78 (d, 2 H, C₆H₄, *J* = 4.0 Hz), 8.63 (d, 1 H, CONH, *J* = 4.4 Hz), 10.11 (s, 1 H, 3-NH), 10.78 (s, 1H, 7-NH).

Diethyl *N*-{4-[5-(2-Amino-4-oxo-4,7-dihydro-3*H*-pyrrolo[2,3-*d*]pyrimidin-6-yl)pentyl]benzoyl}-L-glutamate (13b). Compound **13b** was synthesized as described for **13a**: yield 88% as a yellow syrup, R_f = 0.57 (CHCl₃/MeOH, 5:1). ¹H NMR (DMSO-*d₆*) δ 1.14−1.23 (m, 6 H, 2 CH₃), 1.28−1.38 (m, 2 H, CH₂), 1.55−1.67 (m, 4 H, 2 CH₂), 1.90−2.20 (m, 2 H, CH₂), 2.40−2.68 (m, 6 H, 3 CH₂), 4.02−4.12 (m, 4 H, 2 CH₂), 4.38−4.46 (m, 1 H, CH), 5.85 (s, 1 H, CH), 5.96 (s, 2 H, 2-NH₂), 7.30 (d, 2 H, C₆H₄, *J* = 4.0 Hz), 7.79 (d, 2 H, C₆H₄, *J* = 4.0 Hz), 8.64 (d, 1 H, CONH, *J* = 4.4 Hz), 10.12 (s, 1 H, 3-NH), 10.80 (s, 1H, 7-NH). Anal. (C₂₇H₃₅N₅O₆·0.75H₂O) C, H, N.

Diethyl *N*-{4-[6-(2-Amino-4-oxo-4,7-dihydro-3*H*-pyrrolo[2,3-*d*]pyrimidin-6-yl)hexyl]benzoyl}-L-glutamate (13c). Compound **13c** was synthesized as described for **13a**: 77% yield as a yellow syrup, R_f = 0.60 (CHCl₃/MeOH, 5:1). ¹H NMR (DMSO-*d₆*) δ 1.11−1.21 (m, 6 H, 2 CH₃), 1.25−1.34 (m, 4 H, 2 CH₂), 1.48−1.64 (m, 4 H, 2 CH₂), 1.92−2.16 (m, 2 H, CH₂), 2.39−2.46 (m, 2 H, CH₂), 2.49−2.66 (m, 4 H, 2 CH₂), 4.01−4.14 (m, 4 H, 2 CH₂), 4.37−4.47 (m, 1 H, CH), 5.82 (s, 1 H, CH), 5.94 (s, 2 H, 2-NH₂), 7.28 (d, 2 H, C₆H₄, *J* = 4.0 Hz), 7.78 (d, 2 H, C₆H₄, *J* = 4.0 Hz), 8.63 (d, 1 H, CONH, *J* = 3.8 Hz), 10.10 (s, 1 H, 3-NH), 10.77 (s, 1H, 7-NH). Anal. (C₂₈H₃₇N₅O₆·1.0H₂O) C, H, N.

***N*-{4-[4-(2-Amino-4-oxo-4,7-dihydro-3*H*-pyrrolo[2,3-*d*]pyrimidin-6-yl)butyl]benzoyl}-L-glutamic Acid (3).** To a solution of the diester (**13a**) (580 mg, 1.14mmol) was added 1 N NaOH (15 mL), and the mixture was stirred under N₂ at room temperature for 1 h. TLC showed the disappearance of the starting material (R_f = 0.55) and formation of one major spot at the origin (CHCl₃/MeOH, 5:1). The reaction mixture was evaporated to dryness under reduced pressure. The residue was dissolved in water (10 mL), the resulting solution was cooled in an ice bath, and the pH was adjusted to 3−4 with dropwise addition of 1 N HCl. The resulting suspension was frozen in a dry ice/acetone bath, thawed in a refrigerator to 4−5 °C, and filtered. The residue was washed with a small amount of cold water and ethyl acetate and dried in vacuo using P₂O₅ to afford 380 mg (73%) **3** as a yellow powder: mp 172−173 °C (lit.[23] mp 171−173 °C), R_f = 0.05 (CHCl₃/MeOH, 5:1). ¹H NMR

(DMSO-d_6) δ 1.58 (br, 4 H, 2 CH$_2$), 1.88−2.10 (m, 2 H, CH$_2$), 2.29−2.37 (t, 2 H, CH$_2$), 2.52−2.70 (m, 4 H, 2 CH$_2$), 4.32−4.42 (m, 1 H, CH), 5.83 (s, 1 H, CH), 5.97 (s, 2 H, 2-NH$_2$), 7.26 (d, 2 H, C$_6$H$_4$, J = 4.0 Hz), 7.78 (d, 2 H, C$_6$H$_4$, J = 4.0 Hz), 8.50 (d, 1 H, CONH, J = 3.0 Hz), 10.14 (s, 1 H, 3-NH), 10.78 (s, 1H, 7-NH), 12.21 (br, 2 H, 2 COOH). Anal. (C$_{22}$H$_{25}$N$_5$O$_6$·1.5H$_2$O) C, H, N.

***N*-{4-[5-(2-Amino-4-oxo-4,7-dihydro-3*H*-pyrrolo[2,3-*d*]pyrimidin-6-yl)pentyl]benzoyl}-L-glutamic Acid (4).** Compound **4** was synthesized as described for **3**: yield 60% as a yellow powder, mp 208−209 °C, R_f = 0.05 (CHCl$_3$/MeOH, 5:1). ^{1}H NMR (DMSO-d_6) δ 1.26−1.36 (m, 2 H, CH$_2$), 1.54−1.66 (m, 4 H, 2 CH$_2$), 1.88−2.20 (m, 2 H, CH$_2$), 2.31−2.39 (t, 2 H, CH$_2$), 2.52−2.68 (m, 4 H, 2 CH$_2$), 4.32−4.42 (m, 1 H, CH), 5.85 (s, 1 H, CH), 5.99 (s, 2 H, 2-NH$_2$), 7.29 (d, 2 H, C$_6$H$_4$, J = 4.0 Hz), 7.79 (d, 2 H, C$_6$H$_4$, J = 4.0 Hz), 8.52 (d, 1 H, CONH,, J = 3.9 Hz), 10.14 (s, 1 H, 3-NH), 10.80 (s, 1H, 7-NH), 12.24 (br, 2 H, 2 COOH). Anal. (C$_{23}$H$_{27}$N$_5$O$_6$·1.0H$_2$O) C, H, N.

***N*-{4-[6-(2-Amino-4-oxo-4,7-dihydro-3*H*-pyrrolo[2,3-*d*]pyrimidin-6-yl)hexyl]benzoyl}-L-glutamic Acid (5).** Compound **5** was synthesized as described for **3**: yield 83% as a yellow powder, mp 220−221 °C, R_f = 0.05 (CHCl$_3$/MeOH, 5:1). ^{1}H NMR (DMSO-d_6) δ 1.25−1.35 (m, 4 H, 2 CH$_2$), 1.48−1.65 (m, 4 H, 2 CH$_2$), 1.88−2.15 (m, 2 H, CH$_2$), 2.30−2.38 (t, 2 H, CH$_2$), 2.49−2.68 (m, 4 H, 2 CH$_2$), 4.33−4.43 (m, 1 H, CH), 5.83 (s, 1 H, CH), 5.96 (s, 2 H, 2-NH$_2$), 7.28 (d, 2 H, C$_6$H$_4$, J = 4.0 Hz), 7.90 (d, 2 H, C$_6$H$_4$, J = 4.0 Hz), 8.52 (d, 1 H, CONH,, J = 3.8 Hz), 10.12 (s, 1 H, 3-NH), 10.78 (s, 1H, 7-NH), 12.21 (br, 2 H, 2 COOH). Anal. (C$_{24}$H$_{29}$N$_5$O$_6$·2.5H$_2$O) C, H, N.

Cell Lines and Assays of Antitumor Drug Activities. RFC- and FRα-null MTXRIIOuaR2-4 (R2) Chinese hamster ovary (CHO) cells were a gift from Dr. Wayne Flintoff (University of Western Ontario)[30] and were cultured in α-minimal essential medium (MEM) supplemented with 10% bovine calf serum (Invitrogen, Carlsbad, CA), penicillin-streptomycin solution, and glutamine at 37 °C with 5% CO$_2$. PC43-10 cells are R2 cells transfected with human RFC[31] and were cultured in α-MEM plus 1.5 mg/mL G418. FRα- (designated RT16) and FRβ- (designated D4) expressing CHO cells were derived from R2 cells by electroporation with FRα (obtained from Manohar Ratnam, Medical University of Ohio) and FRβ (prepared by RT-PCR; see Supporting Information) cDNAs in pCDNA3 vector. Cells were cloned, colonies isolated and expanded for screening by Western blots (FRα) or real time RT-PCR (FRβ) (Supporting Information). The RT16 and D4 sublines were maintained as for PC43-10 cells. Prior to the cytotoxicity assays (see below), RT16 and D4 cells were cultured in complete folate-free RPMI 1640 (without added folate) for 3 days. KB human tumor cells were purchased from American Type Culture Collection (ATCC) (Manassas, VA). IGROVI human ovarian cancer cells were provided by Dr. Manohar Ratnam (Medical University of Ohio). Cells were routinely cultured in folate-free RPMI 1640 medium, supplemented with 10% fetal bovine serum, penicillin−streptomycin solution, 2 mM glutamine at 37 °C with 5% CO$_2$.

For growth inhibition assays, cells (CHO, KB, or IGROV1) were plated in 96 well dishes (~5000 cells/well, total volume of 200 μL of medium) with a range of inhibitors including classical antifolates and the 6-substituted pyrrolo[2,3-*d*]pyrimidine antifolates **1**−**5**. The sources of the classical antifolate drugs were as follows: MTX, Drug Development Branch, National Cancer Institute (Bethesda, MD); RTX [*N*-(5-[*N*-(3,4-dihydro-2-methyl-4-oxyquinazolin-6-yl-methyl)-*N*-methylamino]-2-thienoyl)-L-glutamic acid], AstraZeneca Pharmaceuticals (Maccesfield, Cheshire, England); LMX (5,10-dideaza-5,6,7,8-tetrahydrofolate) and PMX [*N*-{4-[2-(2-amino-3,4-dihydro-4-oxo-7*H*-pyrrolo[2,3-*d*]pyrimidin-5-yl)ethyl]benzoyl}-L-glutamic acid] (Alimta), Eli Lilly and Co. (Indianapolis, IN); and BW1843789 [(*S*)-2-(5-(((1,2-dihydro-3-methyl-1-oxo-benzo(*f*)quinazolin-9-yl)methyl)amino)-1-oxo-2-isoindolinyl)glutaric acid], (**5a**) GlaxoWellcome-SmithKline Co. (Research Triangle Park, NC). The culture medium was RPMI 1640 (contains 2.3 μM folic acid) with 10% dialyzed serum and antibiotics for experiments with R2 and PC43-10 cells. For RT-16, D4, KB, and IGROV1 cells, cells were cultured in folate-free RPMI media with 10% dialyzed fetal bovine

serum (Invitrogen) and antibiotics supplemented with 2 nM LCV (Drug Development Branch, National Cancer Institute, Bethesda, MD). The requirement for FR-mediated drug uptake in these assays was established in parallel incubations including 200 nM folic acid (Sigma Chemical Co., St. Louis, MO). Cells were routinely incubated for up to 96 h. Metabolically active cells (a measure of cell viability) were assayed with CellTiter-blue cell viability assay (Promega, Madison, WI), and fluorescence was measured (590 nm emission, 560 nm excitation) with a fluorescence plate reader. Data were exported from Softmax Pro software to an Excel spreadsheet for analysis and determinations of IC$_{50}$ values, corresponding to the drug concentrations that result in 50% loss of cell growth.

For some of the in vitro growth inhibition studies, drug treatments were performed in the presence of higher concentrations (up to 100 nM) of LCV. In others, the inhibitory effects of the antifolate inhibitors on de novo thymidylate biosynthesis (i.e., TS) and de novo purine biosynthesis (GARFTase and AICARFTase) were tested by coincubations with thymidine (10 μM) and adenosine (60 μM). For de novo purine biosynthesis, additional protection experiments used AICA (9.6−192 μM) as a means of distinguishing inhibitory effects at GARFTase from those at AICARFTase.[32]

For assays of colony formation in the presence of the antifolate drugs, KB cells were harvested in log phase and 100 cells were plated into 60 mm dishes in folate-free RPMI1640 medium supplemented with 2 nM LCV, 10% dialyzed fetal bovine serum, penicillin−streptomycin, and 2 mM glutamine, in the presence of antifolate drugs. The dishes were incubated at 37 °C with 5% CO$_2$ for 10 days. At the end of the incubations, the dishes were rinsed with Dulbecco's phosphate buffered saline (DPBS), 5% trichloro-acetic acid, borate buffer (10 mM, pH 8.8), followed by 30 min of incubation in 1% methylene blue in the borate buffer. The dishes were rinsed with the borate buffer, and colonies were enumerated for calculating percent colony-forming efficiency normalized to control.

To test the reversibility of colony-forming inhibition, KB cells were cultured in the presence or absence of 1 μM antifolate compounds for 2 days before rinsing with saline, trypsining, and reinoculating into 60 mm dishes at low and high densities (200 and 400, or 2000 and 4000, cells per dish for cells cultured in absence, or presence of antifolate, respectively). The dishes were incubated for 14 days, and colonies were counted for calculating percent colony-forming efficiency.

FR Binding Assay. [3′,5′,7,9-^{3}H]Folic acid (Moravek Biochemicals, Brea, CA) binding was used to assess levels of surface FRs.[37] Briefly, cells (~1.6 × 10^6) were rinsed twice with DPBS followed by a quick rinse with an acetate buffer (10 mM sodium acetate, 150 mM NaCl, pH 3.5) to remove FR-bound folates. Cells were washed twice with ice-cold Hepes buffered saline (20 mM Hepes, 140 mM NaCl, 5 mM KCl, 2 mM MgCl$_2$, 5 mM glucose, pH7.4) (HBS). Cells were incubated in HBS with [^{3}H]folic acid (50 nM, specific activity 0.5 Ci/mmol) in the presence and absence of unlabeled folic acid or antifolate for 15 min at 0 °C. The dishes were rinsed three times with ice-cold HBS, after which the cells were solubilized with 0.5 N sodium hydroxide and aliquots measured for radioactivity and protein contents. Protein assays were performed by the method of Lowry et al.[38] Bound [^{3}H]folic acid was calculated as pmol/mg protein. Total FR levels for different cell lines (KB, IGROV1, R2, PC43-10, RT16, D4) were calculated from the differences in pmol/mg of bound [^{3}H]folic acid in the absence and presence of excess (5 μM) unlabeled folic acid. Relative binding affinities for assorted folate/antifolate substrates were determined over a range of ligand concentrations and were calculated as the inverse molar ratio of unlabeled ligands required to inhibit [^{3}H]folic acid binding by 50%. By definition, the relative affinity of folic acid is 1.

Transport Assays for RFC. For monolayer cultures of different cell lines (KB, IGROV1, R2, PC43-10, RT16, D4), RFC transport capacity was assayed by measuring the uptake of 0.5 μM [3′, 5′, 7-^{3}H] MTX (Moravek Biochemicals) over 2 min at 37 °C in 2 mL of anion-free Hepes−sucrose−Mg^{2+} buffer (HSM buffer, 20 mM Hepes, 235 mM sucrose, pH adjusted to 7.14 with MgO) in 60

mm culture dishes. Uptake of [³H]MTX was quenched with ice-cold DPBS. Cells were washed with ice-cold DPBS (3×) and solubilized with 0.5 N NaOH. Levels of intracellular radioactivity were expressed as pmol/mg protein, calculated from direct measurements of radioactivity and protein contents of cell homogenates. Protein assays were based on the method of Lowry et al.[38] For experiments to determine the inhibitions of hRFC transport by the pyrrolopyrimidine analogues and several classical antifolate compounds, transport was measured with PC43-10 cells in a similar assay, but in physiologic Hank's balanced salt solution (HBSS), with [³H]MTX (0.5 μM) in the presence and absence of unlabeled antifolates (10 μM) over 2 min at 37 °C.[30]

In Situ GARFT Enzyme Inhibition Assay. Incorporation of [¹⁴C(U)]glycine (Moravek Biochemicals) into [¹⁴C]formyl GAR as an in situ measure of endogenous GARFTase activity was described by Beardsley et al.[32] for studies with the GARFTase inhibitor LMX. For these experiments, KB cells were seeded in 4 mL of complete folate-free RPMI 1640 plus 2 nM LCV in 60 mm dishes at a density of 2×10^6 cells per dish. On the next day, the medium was replaced with 2 mL of fresh complete folate-free RPMI 1640 plus 2 nM LCV (without supplementing glutamine). Azaserine (4 μM final concentration) was added in the presence and absence of the antifolate inhibitors (0.1, 1, 10, 100, 1000 nM). After 30 min, glutamine (final concentration, 2 mM) and [¹⁴C]glycine (final specific activity 0.1 mCi/L) were added. Incubations were at 37 °C for 15 h, at which time cells were washed (one time) with ice-cold folate-free RPMI 1640 plus serum. Cell pellets were dissolved in 2 mL of 5% trichloroacetic acid at 0 °C. Cell debris was removed by centrifugation (the cell protein contents in the pellets was measured), and the supernatants were extracted twice with 2 mL of ice-cold ether. The aqueous layer was passed through a 1 cm column of AG1x8 (chloride form), 100−200 mesh (Bio-Rad), washed with 10 mL of 0.5 N formic acid, followed by 10 mL of 4 N formic acid, and eluted with 8 mL of 1 N HCl solution. The elutants were collected and determined for radioactivity. The accumulation of radioactive formyl GAR was calculated as pmol/mg protein over a range of inhibitor concentrations.

In Vitro GARFT Enzyme Inhibition Assay. Purified recombinant mouse GARFT enzyme, α,β-GAR, and coenzyme 10-formyl-5,8-dideazafolic acid were gifts from Dr. Richard Moran (Virginia Commonwealth University, Richmond, VA).[39] Enzyme activity was assayed spectrophotometrically at 37 °C using GARFTase (0.75 nM), α,β-GAR (11 μM), and 10-formyl-5,8-dideazafolic acid (10 μM) in HEPES buffer (75 mM, pH 7.5) with or without antifolate inhibitor (10 to 30 000 nM). The absorbance of the reaction product, 5,8-dideazafolic acid, was monitored at 295 nM over the first minute as a measure of the initial rate of enzyme activity. IC_{50} values were calculated as the concentrations of inhibitors that resulted in 50% decrease in the initial velocity of the enzymatic reaction.

Apoptosis Assays. KB cells were cultured in the presence or absence of 1 μM antifolate compounds, or daunorubicin as positive control, for 24 h. Cells were collected by trypsinization and resuspended to a density of ∼10⁶ cells/mL. Cells were stained with a annexin V-FITC kit according to the manufacturer's instructions (Beckman-Coulter, Fullerton, CA) and analyzed with a EPICS-XL MCL flow cytometer (Beckman-Coulter) equipped with an argon laser. Viable intact cells were gated based on FS/SS characteristics, and annexin V-FITC staining was measured. Percent apoptosis was calculated as the percent of Annexin V-FITC stained cells out of the total viable cells.

Supporting Information Available: Additional experimental details on the development of CHO (Chinese hamster ovary) subline expressing human folate receptors (FR) and α and β; elemental analysis results. This material is available free of charge via the Internet at http://pubs.acs.org.

References

(1) Stokstad, E. L. R. Historical Perspective on Key Advances in the Biochemistry and Physiology of Folates. In *A Folic Acid Metabolism in Health and Disease*; Picciano, M. F., Stokstad, E. L. R., Greogory, J. F. Eds.; Wiley-Liss: New York, 1990; pp 1−21.

(2) Matherly, L. H.; Goldman, I. D. Membrane Transport of Folates. *Vitam. Horm.* **2003**, *66*, 403–456.

(3) Matherly, L. H.; Hou, Z.; Deng, Y. Human Reduced Folate Carrier: Translation of Basic Biology to Cancer Etiology and Therapy. *Cancer Metastasis Rev.* **2007**, *26*, 111–128.

(4) Zhao, R.; Goldman, I. D. Resistance to Antifolates. *Oncogene* **2003**, *22*, 7431–7457.

(5) Qiu, A.; Jansen, M.; Sakaris, A.; Min, S. H.; Chattopadhyay, S.; Tsai, E.; Sandoval, C.; Zhao, R.; Akabas, M. H.; Goldman, I. D. Identification of an Intestinal Folate Transporter and the Molecular Basis for Hereditary Folate Malabsorption. *Cell* **2006**, *127*, 917–928.

(6) Salazar, M. D.; Ratnam, M. The Folate Receptor: What Does It Promise in Tissue-Targeted Therapeutics? *Cancer Metastasis Rev.* **2007**, *26*, 141–152.

(7) Hilgenbrink, A. R.; Low, P. S. Folate Receptor-Mediated Drug Targeting: From Therapeutics to Diagnostics. *J. Pharm. Sci.* **2005**, *94*, 2135–2146.

(8) Ragoussis, J.; Senger, G.; Trowsdale, J.; Campbell, I. G. Genomic Organization of the Human Folate Receptor Genes on Chromosome 11q13. *Genomics* **1992**, *14*, 423–430.

(9) Spiegelstein, O.; Eudy, J. D.; Finnell, R. H. Identification of Two Putative Novel Folate Receptor Genes in Humans and Mouse. *Gene* **2000**, *258*, 117–125.

(10) Wang, X.; Shen, F.; Freisheim, J. H.; Gentry, L. E.; Ratnam, M. Differential Stereospecificities and Affinities of Folate Receptor Isoforms for Folate Compounds and Antifolates. *Biochem. Pharmacol.* **1992**, *44*, 1898–1901.

(11) Toffoli, G.; Cernigoi, C.; Russo, A.; Gallo, A.; Bagnoli, M.; Boiocchi, M. Overexpression of Folate Binding Protein in Ovarian Cancers. *Int. J. Cancer* **1997**, *74*, 193–198.

(12) Wu, M.; Gunning, W.; Ratnam, M. Expression of Folate Receptor Type Alpha in Relation to Cell Type, Malignancy, and Differentiation in Ovary, Uterus, and Cervix. *Cancer Epidemiol., Biomarkers Prev.* **1999**, *8*, 775–782.

(13) Pan, X. Q.; Zheng, X.; Shi, G.; Wang, H.; Ratnam, M.; Lee, R. J. Strategy for the Treatment of Acute Myelogenous Leukemia Based on Folate Receptor Beta-Targeted Liposomal Doxorubicin Combined with Receptor Induction Using All-Trans Retinoic Acid. *Blood* **2002**, *100*, 594–602.

(14) Reddy, J. A.; Haneline, L. S.; Srour, E. F.; Antony, A. C.; Clapp, D. W.; Low, P. S. Expression and Functional Characterization of the Beta-Isoform of the Folate Receptor on CD34(+) Cells. *Blood.* **1999**, *93*, 3940–3948.

(15) Jansen, G. Receptor- and Carrier-Mediated Transport Systems for Folates and Antifolates. Exploitation for Folate Chemotherapy and Immunotherapy. In *Anticancer Development Guide: Antifolate Drugs in Cancer Therapy*; Jackman, A. L. Ed.; Humana Press Inc.: Totowa, NJ, 1999; pp 293−321.

(16) Jackman, A. L.; Theti, D. S.; Gibbs, D. D. Antifolates Targeted Specifically to the Folate Receptor. *Adv. Drug Delivery Rev.* **2004**, *56*, 1111–1125.

(17) Ray, M. S.; Muggia, F. M.; Leichman, C. G.; Grunberg, S. M.; Nelson, R. L.; Dyke, R. W.; Moran, R. G. Phase I Study of (6R)-5,10-dideazatetrahydrofolate: A Folate Antimetabolite Inhibitory to de Novo Purine Synthesis. *J. Natl. Cancer Inst.* **1993**, *85*, 1154–1159.

(18) Reddy, J. A.; Westrick, E.; Vlahov, I.; Howard, S. J.; Santhapuram, H. K.; Leamon, C. P. Folate Receptor Specific Anti-Tumor Activity of Folate−Mitomycin Conjugates. *Cancer Chemother. Pharmacol.* **2006**, *58*, 229–236.

(19) Theti, D. S.; Bavetsias, V.; Skelton, L. A.; Titley, J.; Gibbs, D.; Jansen, G.; Jackman, A. L. Selective Delivery of CB300638, a Cyclo-penta[*g*]quinazoline-Based Thymidylate Synthase Inhibitor into Human Tumor Cell Lines Overexpressing the Alpha-Isoform of the Folate Receptor. *Cancer Res.* **2003**, *63*, 3612–3618.

(20) Gibbs, D. D.; Theti, D. S.; Wood, N.; Green, M.; Raynaud, F.; Valenti, M.; Forster, M. D.; Mitchell, F.; Bavetsias, V.; Henderson, E.; Jackman, A. L. BGC 945, a Novel Tumor-Selective Thymidylate Synthase Inhibitor Targeted to Alpha-Folate Receptor-Overexpressing Tumors. *Cancer Res.* **2005**, *65*, 11721–11728.

(21) Shih, C.; Barnett, C. J.; Grindey, G. B.; Pearce, H. L.; Engelhardt, J. A.; Todd, G. C.; Rinzel, S. M.; Worzalla, J. F.; Gossett, L. S.;

Everson, T. P.; Wilson, T. M.; Kobierski, M. E.; Winter, M. A.; Moran, R. G.; Kuhnt, D.; Taylor, E. C. Structural Features That Determine the Biological Activity of Pyrrolo[2,3-*d*]pyrimidine Based Antifolates. Presented at the 10th International Symposium, Chemistry and Biology of Pteridines and Folates, Orange Beach, AL, March 21–26, 1993; Abstract F15.

(22) Gangjee, A.; Zeng, Y.; McGuire, J. J.; Mehraein, F.; Kisliuk, R. L. Synthesis of Classical, Three-Carbon-Bridged 5-Substituted Furo[2,3-*d*]pyrimidine and 6-Substituted Pyrrolo[2,3-*d*]pyrimidine Analogues as Antifolates. *J. Med. Chem.* **2004**, *47*, 6893–6901.

(23) Gangjee, A.; Zeng, Y.; McGuire, J. J.; Kisliuk, R. L. Synthesis of Classical, Four-Carbon Bridged 5-Substituted Furo[2,3-*d*]pyrimidine and 6-Substituted Pyrrolo[2,3-*d*]pyrimidine Analogues as Antifolates. *J. Med. Chem.* **2005**, *48*, 5329–5336.

(24) Baldwin, S. W.; Tse, A.; Gossett, L. S.; Taylor, E. C.; Rosowsky, A.; Shih, C.; Moran, R. G. Structural Features of 5,10-Dideaza-5,6,7,8-tetrahydrofolate That Determine Inhibition of Mammalian Glycinamide Ribonucleotide Formyltransferase. *Biochemistry* **1991**, *30*, 1997–2006.

(25) Gangjee, A.; Yang, J.; McGuire, J. J.; Kisliuk, R. L. Synthesis and Evaluation of a Classical 2,4-Diamino-5-substituted-furo[2,3-*d*]pyrimidine and a 2-Amino-4-oxo-6-substituted-pyrrolo[2,3-*d*]pyrimidine as Antifolates. *Bioorg. Med. Chem.* **2006**, *14*, 8590–8598.

(26) Secrist, J. A., III; Liu, P. S. Studies Directed Toward a Total Synthesis of Nucleoside Q. The Annulation of 2,6-Diaminopyrimidin-4-one with α-Halo Carbonyls to Form Pyrrolo[2,3-*d*]pyrimidines and Furo[2,3-*d*]pyrimidines. *J. Med. Chem.* **1978**, *43*, 3937–3941. In the original report of the condensation of α-bromomethylketones, Secrist and Lu obtained only the pyrrolo[2,3-*d*]pyrimidines in all cases except one where both the pyrrolo- and furo[2,3-*d*]pyrimidines were obtained. This indicates that since the pyrimidine precursor is constant, the variation in the product composition must be due to the halo ketone.

(27) Salley, J. J.; Glennon, R. A. Studies on Simplified Ergoline Derivatives. A General Six-Step Synthesis of Phenyl-Substituted 4-Methyl-3,4,4a,5,6,10b-hexahydrobenzo-[*f*]quinolin-1-(2*h*)-one Analogues (1). *J. Heterocycl. Chem.* **1982**, *19*, 545–550.

(28) Gangjee, A.; Yang, J.; Ihnat, M. A.; Kamat, S. Antiangiogenic and Antitumor Agents: Design, Synthesis and Evaluation of Novel 2-Amino-4-(3-bromoanilino)-6-benzyl Substituted Pyrrolo[2,3-*d*]pyrimidines as Inhibitors of Receptor Tyrosine Kinases. *Bioorg. Med. Chem.* **2003**, *11*, 5155–5170.

(29) Taylor, E. C.; Young, W. B.; Spanka, C. Synthesis of *N*-{4-[2-(2-Amino-5,6-dihydro-4(3*H*)-oxo-7H-pyrrolo[2,3-*d*]pyrimidin-6-yl)eth-yl]benzoyl}-L-glutamic Acid: A Ring-Contracted Analog of 5,10-Dideaza-5,6,7,8-tetrahydrofolic Acid. *J. Org. Chem.* **1996**, *61*, 1261–1266.

(30) Flintoff, W. F.; Davidson, S. V.; Siminovitch, L. Isolation and Partial Characterization of Three Methotrexate-Resistant Phenotypes from Chinese Hamster Ovary Cells. *Somatic Cell Genet.* **1976**, *2*, 245–261.

(31) Wong, S. C.; Proefke, S. A.; Bhushan, A.; Matherly, L. H. Isolation of Human cDNAs that Restore Methotrexate Sensitivity and Reduced Folate Carrier Activity in Methotrexate Transport Defective Chinese Hamster Ovary Cells. *J. Biol. Chem.* **1995**, *270*, 17468–17475.

(32) Beardsley, G. P.; Moroson, B. A.; Taylor, E. C.; Moran, R. G. A New Folate Antimetabolite, 5,10-Dideaza-5,6,7,8-tetrahydrofolate Is a Potent Inhibitor of de Novo Purine Synthesis. *J. Biol. Chem.* **1989**, *264*, 328–333.

(33) Goldman, I. D.; Zhao, R. Molecular, Biochemical, and Cellular Pharmacology of Pemetrexed. *Semin. Oncol.* **2002**, *29*, 3–17.

(34) Tonkinson, J. L.; Marder, P.; Andis, S. L.; Schultz, R. M.; Gossett, L. S.; Shih, C.; Mendelsohn, L. G. Cell Cycle Effects of Antifolate Antimetabolites: Implications for Cytotoxicity and Cytostasis. *Cancer Chemother. Pharmacol.* **1997**, *39*, 521–531.

(35) Smith, S. G.; Lehman, N. L.; Moran, R. G. Cytotoxicity of Antifolate Inhibitors of Thymidylate and Purine Synthesis to WiDr Colonic Carcinoma Cells. *Cancer Res.* **1993**, *53*, 5697–5706.

(36) Barbour, K. W.; Berger, F. G. Cell Death in Response to Antimetabolites Directed at Thymidylate Synthase. *Cancer Chemother. Pharmacol.* **2008**, *61*, 189–201.

(37) Chattopadhyay, S.; Wang, Y.; Zhao, R.; Goldman, I. D. Lack of Impact of the Loss of Constitutive Folate Receptor Alpha Expression, Achieved by RNA Interference, on the Activity of the New Generation Antifolate Pemetrexed in HeLa Cells. *Clin. Cancer Res.* **2004**, *10*, 7986–7993.

(38) Lowry, O. H.; Rosebrough, N. J.; Farr, A. L.; Randall, R. J. Protein Measurement with the Folin Phenol Reagent. *J. Biol. Chem.* **1951**, *193*, 265–275.

(39) Sanghani, S. P.; Moran, R. G. Tight Binding of Folate Substrates and Inhibitors to Recombinant Mouse Glycinamide Ribonucleotide Formyltransferase. *Biochemistry* **1997**, *36*, 10506–10516.